

**UCLA**  
**COMPUTATIONAL AND APPLIED MATHEMATICS**

---

**Weighted Essentially Non-Oscillatory Schemes**

**Xu-Dong Liu**  
**Stanley Osher**  
**Tony Chan**

**July 1993**

**CAM Report 93-22**

---

**Department of Mathematics**  
**University of California, Los Angeles**  
**Los Angeles, CA. 90024-1555**

# Weighted Essentially Non-Oscillatory Schemes

Xu-Dong Liu\*    Stanley Osher†    Tony Chan‡

---

\*Department of Mathematics, UCLA, Los Angeles, California, 90024. Research supported by NSF grant DMS 91-04311.

†Department of Mathematics, UCLA, Los Angeles, California, 90024. Research supported by NSF DMS 91-03104 and ONR NOO014-92-J-1890

‡Department of Mathematics, UCLA, Los Angeles, California, 90024. Research supported by NSF ASC90-91-03002, ARO DAAL03- 91-G-150 and ONR NOO014-90-J-1695

Running head: Weighted ENO Schemes

Proofs sent to:

Xu-Dong Liu

Department of Mathematics, UCLA

Los Angeles, CA 90024

AMS(MOS) subject classifications: Primary 65M10; Secondary 65M05

Keywords: Hyperbolic Conservation Laws, ENO

## Abstract

In this paper we introduce a new version of ENO (Essentially Non-Oscillatory) shock-capturing schemes which we call Weighted ENO. The main new idea is that, instead of choosing the “smoothest” stencil to pick one interpolating polynomial for the ENO reconstruction, we use a convex combination of all candidates to achieve the essentially non-oscillatory property, while additionally obtaining one order of improvement in accuracy. The resulting Weighted ENO schemes are based on cell-averages and a TVD Runge-Kutta time discretization. Preliminary encouraging numerical experiments are given.

# 1 Introduction

In this paper we present a new version of ENO ( Essentially Non-Oscillatory ) schemes. The cell-average version of ENO schemes originally was introduced and developed by Harten and Osher in [1] and Harten, Engquist, Osher and Chakravarthy in [2]. Later Shu and Osher developed the flux version of ENO schemes and introduced the TVD Runge-Kutta time discretization in [3] and [4]. The ENO schemes work well in many numerical experiments. The new ENO schemes which we call the Weighted ENO schemes are based on cell-averages and the TVD Runge-Kutta time discretization.

The only difference between these schemes and the standard cell-average version of ENO is how we define a reconstruction procedure which produces a high-order accurate global approximation to the solution from its given cell-averages. The cell-average version of ENO schemes attempts to avoid growth of spurious oscillations by an adaptive-stencil approach, in which each cell is assigned its own stencil of cells for the purposes of reconstruction. For each cell the cell-average version of ENO schemes selects an interpolating stencil in which the solution is smoothest in some sense. Thus a cell near a discontinuity is assigned a stencil from the smooth part of the solution and a Gibbs-like phenomenon is so avoided ( see [5] ). The Weighted ENO schemes developed here follow this basic idea by using a convex combination approach, in which each cell is assigned all corresponding stencils and a convex combination of all corresponding interpolating polynomials on the stencils is computed to be the approximating polynomial. This is done by assigning proper weights to the convex combination. To achieve the essentially non-oscillatory property as the cell-average version of ENO, the Weighted ENO schemes require that the convex combination be essentially a convex combination of the interpolating polynomials on the smooth stencils and that the interpolating polynomials on the discontinuous stencils have essentially no contribution to the convex combination. Thus, as in the cell-average version of ENO schemes, a cell near a discontinuity is essentially assigned stencils from the smooth part of the solution and a Gibbs-like phenomenon is also avoided. In addition to this, the convex combination approach results in cancellation of truncation errors of corresponding interpolating polynomials and achieve one order of improvement in accuracy. Another possible advantage of Weighted ENO is smoother dependence of data which may lessen some of ENO's oscillatory behavior near convergence and may help in getting a convergence proof.

In §2 we introduce some notations and basic notions and give the TVD Runge-Kutta time discretization. In §3 we describe the procedure of reconstruction from given cell averages. In §4 we present some preliminary numerical experiments.

## 2 Basic Formulation and TVD Runge-Kutta Time Discretization

We consider a hyperbolic conservation law

$$\begin{aligned} u_t + f(u)_x &= 0, \\ u(x, 0) &= u_o(x). \end{aligned} \tag{2.1}$$

Following the basic ENO framework originating in [2], we let  $\{I_j \times [t_n, t_{n+1}]\}$  be a partition of  $R \times [0, T]$ , where  $I_j = [x_{j-\frac{1}{2}}, x_{j+\frac{1}{2}}]$  is the  $j$ -th cell,  $x_j = j \cdot h$ ,  $t_n = n \cdot \tau$ , and  $T$  is the stopping time. We denote  $\{\bar{u}(x_j, t)\}$  to be the sliding averages of the weak solution  $u(x, t)$  of (2.1) i.e.

$$\bar{u}(x_j, t) = \frac{1}{h} \int_{I_j} u(x, t) dx. \tag{2.2}$$

Integrating (2.1) on the  $j$ -th cell  $I_j$ , we obtain that the sliding averages  $\{\bar{u}(x_j, t)\}$  of the weak solution  $u(x, t)$  of (2.1) satisfy

$$\begin{aligned} \frac{\partial}{\partial t} \bar{u}(x_j, t) &= \Phi_j(u) \\ &= -\frac{1}{h} [f(u(x_{j+\frac{1}{2}}, t)) - f(u(x_{j-\frac{1}{2}}, t))]. \end{aligned} \tag{2.3}$$

For evaluating  $\Phi_j(u)$ , we need to evaluate  $f(u(x_{j+\frac{1}{2}}, t))$  and  $f(u(x_{j-\frac{1}{2}}, t))$ . First of all, from given cell-averages  $\bar{u} = \{\bar{u}_j\}$  in which  $\bar{u}_j$  approximates  $\bar{u}(x_j, t)$ , we reconstruct the solution to obtain  $R(x, \bar{u}) = \{R_j(x, \bar{u})\}$  which is a piecewise polynomial with uniform polynomial degree  $r - 1$ , and in which each  $R_j(x, \bar{u})$  is a polynomial approximating  $u(x, t)$  on  $I_j$ . We shall show how to get  $R(x, \bar{u})$  from  $\bar{u} = \{\bar{u}_j\}$  in §3. Next at each interface between adjacent cells,  $R(x, \bar{u})$  may have two approximating values  $R_j(x_{j+\frac{1}{2}}, \bar{u})$  and  $R_{j+1}(x_{j+\frac{1}{2}}, \bar{u})$  for  $u(x_{j+\frac{1}{2}}, t)$ . Here we need a two-point Lipschitz monotone flux  $\tilde{h}(\cdot, \cdot)$  which is nondecreasing for the first argument and nonincreasing for the second argument. Some possible choices are

(i) Engquist-Osher

$$h^{EO}(a, b) = \int_0^b \min(f'(s), 0) ds + \int_0^a \max(f'(s), 0) ds + f(0); \quad (2.4)$$

(ii) Godunov

$$h^G(a, b) = \begin{cases} \min_{a \leq u \leq b} f(u) & \text{if } a \leq b, \\ \max_{a \geq u \geq b} f(u) & \text{if } a > b; \end{cases} \quad (2.5)$$

(iii) Roe with entropy fix

$$h^{RF}(a, b) = \begin{cases} f(a) & \text{if } f'(u) \geq 0 \text{ for } u \in [\min(a, b), \max(a, b)], \\ f(b) & \text{if } f'(u) \leq 0 \text{ for } u \in [\min(a, b), \max(a, b)], \\ h^{LLF}(a, b) & \text{otherwise,} \end{cases} \quad (2.6a)$$

where  $h^{LLF}(a, b)$  is defined as

$$h^{LLF}(a, b) = \frac{1}{2}[f(a) + f(b) - \beta(b - a)], \quad \beta = \max_{\min(a, b) \leq u \leq \max(a, b)} |f'(u)|. \quad (2.6b)$$

Finally we can approximate  $f(u(x_{j+\frac{1}{2}}, t))$  by  $\tilde{h}(R_j(x_{j+\frac{1}{2}}), R_{j+1}(x_{j+\frac{1}{2}}))$  and  $f(u(x_{j-\frac{1}{2}}, t))$  by  $\tilde{h}(R_{j-1}(x_{j-\frac{1}{2}}), R_j(x_{j-\frac{1}{2}}))$ .

Hence we can obtain a numerical spatial operator  $L_j(\bar{u})$  approximating the spatial operators  $\Phi_j(u)$  at each cell and

$$\begin{aligned} \frac{\partial}{\partial t} \bar{u}(x_j, t) &= \Phi_j(u) \\ &= -\frac{1}{h}[f(u(x_{j+\frac{1}{2}}, t)) - f(u(x_{j-\frac{1}{2}}, t))] \\ &= L_j(\bar{u}) + O(h^{r+1}) \quad (\text{in most cells}), \end{aligned} \quad (2.7a)$$

where

$$L_j(\bar{u}) = -\frac{1}{h}[\tilde{h}(R_j(x_{j+\frac{1}{2}}), R_{j+1}(x_{j+\frac{1}{2}})) - \tilde{h}(R_{j-1}(x_{j-\frac{1}{2}}), R_j(x_{j-\frac{1}{2}}))]. \quad (2.7b)$$

*Remark 1:* Normally, we only can obtain  $\Phi_j(u) = L_j(\bar{u}) + O(h^r)$ , because we only use polynomials of degree  $r - 1$  to approximate  $u(x, t)$ . In general upwind schemes, away from sonic points where  $f'(u) = 0$ ,  $\tilde{h}(a, b)$  will be either  $f(a)$  or  $f(b)$ . In (2.7b) we need  $R_j(x, \bar{u})$  only at the end points of cells, and in the reconstruction procedure we shall describe, in smooth regions of  $u(x, t)$ ,

$$u(x_j^*, t) = R_j(x_j^*, \bar{u}) + O(h^{r+1}), \quad (2.8)$$

where, in general,  $x_j^*$  is the appropriate one of two end points of  $I_j$ , and hence

$$\begin{aligned}\tilde{h}(R_j(x_{j+\frac{1}{2}}), R_{j+1}(x_{j+\frac{1}{2}})) &= f(u(x_{j+\frac{1}{2}}, t)) + O(h^{r+1}), \\ \tilde{h}(R_{j-1}(x_{j-\frac{1}{2}}), R_j(x_{j-\frac{1}{2}})) &= f(u(x_{j-\frac{1}{2}}, t)) + O(h^{r+1}), \\ L_j(\bar{u}) &= \Phi_j(u) + O(h^{r+1}).\end{aligned}$$

We can now evaluate  $\frac{\partial}{\partial t}\bar{u}(x_j, t)$  numerically. For high order time discretization accuracy, we shall apply an  $(r + 1)$ -th order TVD Runge-Kutta time discretization introduced by Shu and Osher in [3] combined with the Weighted ENO schemes as follows: Let  $\bar{u}^0 = \{\bar{u}_0(x_j)\}$  and for  $n = 0, 1, 2, \dots$ . We compute:

$$\begin{aligned}\bar{u}^{(0)} &= \bar{u}^n, \\ \bar{u}^{(i)} &= \sum_{k=0}^{i-1} [\alpha_{ik}\bar{u}^{(k)} + \beta_{ik}\tau L_j(\bar{u}^{(k)})], \quad i = 1, 2, \dots, \bar{r}, \\ \bar{u}^{n+1} &= \bar{u}^{(\bar{r})},\end{aligned}\tag{2.9}$$

where all  $\bar{u} = \{\bar{u}_j\}$  approximate the cell averages  $\{\bar{u}(x_j, t)\}$  of the weak solution  $u(x, t)$  at corresponding time  $t$ . Here we have  $\bar{r} = 3$ , if  $r + 1 = 3$ , and  $\bar{r} = 4$ , if  $r + 1 = 4$ . Some of the schemes are listed in following Table. If  $\beta_{ik} < 0$  which happens for  $\bar{r} \geq 4$ , then we use  $\tilde{L}_j(\bar{u})$  instead of  $L_j(\bar{u})$ , but in this paper we set  $\tilde{L}_j(\bar{u}) = L_j(\bar{u})$ . For details see [3].

**TVD Runge-Kutta Schemes**

Order	$\alpha_{ik}$	$\beta_{ik}$	CFL
3	$\alpha_{10} = 1$ $\alpha_{20} = \frac{3}{4}, \alpha_{21} = \frac{1}{4}$ $\alpha_{30} = \frac{1}{3}, \alpha_{31} = 0, \alpha_{32} = \frac{2}{3}$	$\beta_{10} = 1$ $\beta_{20} = 0, \beta_{21} = \frac{1}{4}$ $\beta_{30} = 0, \beta_{31} = 0, \beta_{32} = \frac{2}{3}$	1
4	$\alpha_{10} = 1$ $\alpha_{20} = \frac{1}{2}, \alpha_{21} = \frac{1}{2}$ $\alpha_{30} = \frac{1}{3}, \alpha_{31} = \frac{2}{3}, \alpha_{32} = \frac{2}{3}$ $\alpha_{40} = 0, \alpha_{41} = \frac{1}{3}, \alpha_{42} = \frac{1}{3}, \alpha_{43} = \frac{1}{3}$	$\beta_{10} = \frac{1}{2}$ $\beta_{20} = \frac{-1}{4}, \beta_{21} = \frac{1}{2}$ $\beta_{30} = \frac{-1}{9}, \beta_{31} = \frac{-1}{3}, \beta_{32} = 1$ $\beta_{40} = 0, \beta_{41} = \frac{1}{6}, \beta_{42} = 0, \beta_{43} = \frac{1}{6}$	$\frac{2}{3}$

To complete the construction of our schemes we form our novel reconstruction procedure.



## 3 The Reconstruction Procedure

### 3.1 The Purposes of the Reconstruction

In this section we present the reconstruction procedure which we shall use to obtain a piecewise polynomial  $R(x, \bar{u}) = \{R_j(x, \bar{u})\}$  where each  $R_j(x, \bar{u})$  is a polynomial of degree  $r - 1$  approximating the weak solution  $u(x, t)$  in the  $j$ -th cell  $I_j$ . The  $R(x, \bar{u})$  is required to satisfy

(i) In each cell  $I_j$ ,  $\forall x \in I_j$  and any given  $x_j^* \in I_j$ , we have

$$R_j(x, \bar{u}) = u(x, t) + O(h^r), \quad (3.1a)$$

and

$$R_j(x_j^*, \bar{u}) = u(x_j^*, t) + O(h^{r+1}), \quad (3.1b)$$

in smooth regions of  $u(x, t)$ , where (3.1b) will lead to one order of improvement in accuracy, see subsection 3.4 in this paper.

(ii)  $R(x, \bar{u})$  has conservation form i.e.  $\forall j$

$$\frac{1}{h} \int_{I_j} R_j(x, \bar{u}) dx = \bar{u}_j. \quad (3.2)$$

(iii) Every  $R_j(x, \bar{u})$  achieves the “ENO property” which will be specified later.

### 3.2 The Interpolation on Each Stencil

Following the reconstruction procedure in [2], given the cell averages  $\{\bar{u}_j\}$ , we can immediately evaluate the point values of the solution’s primitive function  $W(x)$  at interfaces between the cells  $\{W(x_{j+\frac{1}{2}})\}$ , where the primitive function is defined as

$$W(x) = \int_x^x u(x, t) dx, \quad (3.3)$$

hence

$$u(x, t) = \frac{d}{dx} W(x), \quad (3.4)$$

and obviously

$$W(x_{j+\frac{1}{2}}) = \sum_{i=i'}^j \bar{u}_i \cdot h. \quad (3.5)$$

To reconstruct the solution, for each stencil  $S_j = (x_{j-r+\frac{1}{2}}, x_{j-r+\frac{3}{2}}, \dots, x_{j+\frac{1}{2}})$ , we interpolate  $W(x)$  on  $S_j$  to obtain a polynomial  $p_j(x)$  i.e.

$$p_j(x_{l+\frac{1}{2}}) = W(x_{l+\frac{1}{2}}), \quad l = j - r, \dots, j.$$

Obviously the corresponding polynomial  $\frac{d}{dx}p_j(x)$  approximates the solution  $u(x, t)$  i.e.

$$u(x, t) = \frac{d}{dx}p_j(x) + O(h^r) \quad \forall x \in (x_{j-r+\frac{1}{2}}, x_{j+\frac{1}{2}}),$$

in smooth regions of  $u(x, t)$ , where  $\frac{d}{dx}p_j(x)$  is the interpolating polynomial with degree  $r - 1$ , see [2].

Also for each stencil  $S_j = (x_{j-r+\frac{1}{2}}, x_{j-r+\frac{3}{2}}, \dots, x_{j+\frac{1}{2}})$ , we will define an indicator of the smoothness  $IS_j$  of  $u(x, t)$  on  $S_j$  as following: First we compute a table of differences of  $\{u_j\}$  on  $S_j$ ,

$$\begin{aligned} & \Delta[u_{j-r+1}], \Delta[u_{j-r+2}], \dots, \Delta[u_{j-1}], \\ & \Delta^2[u_{j-r+1}], \Delta^2[u_{j-r+2}], \dots, \Delta^2[u_{j-2}], \\ & \vdots \\ & \Delta^{r-1}[u_{j-r+1}], \end{aligned}$$

where

$$\Delta[u_l] = u_{l+1} - u_l$$

is a difference operator. Next we define  $IS_j$  to be the summation of all averages of absolute values of the same order differences.

$$IS_j = \sum_{l=1}^{r-1} \left( \sum_{k=1}^l |\Delta^{r-l}[u_{j-r+k}]| \right) / l.$$

That is for  $r = 2$ ,

$$IS_j = |\Delta[u_{j-1}]|;$$

and for  $r = 3$ ,

$$IS_j = (|\Delta[u_{j-2}]| + |\Delta[u_{j-1}]|) / 2 + |\Delta^2[u_{j-2}]|.$$

We observe that if  $u(x, t)$  is discontinuous on  $S_j$ ,  $IS_j \approx O(1)$ , and if  $u(x, t)$  is continuous on  $S_j$ ,  $IS_j \approx O(h)$ .

Hence for each stencil  $S_j$ , we obtain  $\frac{d}{dx}p_j(x)$  approximating  $u(x, t)$  on  $S_j$  and  $IS_j$  indicating the smoothness of  $u(x, t)$  on  $S_j$ .

In the following subsection, to reconstruct the solution in  $I_j$ , we shall use  $r$  interpolating polynomials  $\{\frac{d}{dx}p_{j+k}(x)\}_{k=0}^{r-1}$  on the stencils  $\{S_{j+k}\}_{k=0}^{r-1}$  which cover the  $I_j$  to obtain a convex combination of them, and we shall explore  $\{IS_{j+k}\}_{k=0}^{r-1}$  to assign a proper weight for each of  $\{\frac{d}{dx}p_{j+k}(x)\}_{k=0}^{r-1}$  in the convex combination for the purposes of reconstruction.

### 3.3 The Convex Combination of $p_j(x)$ on Each Cell

For each cell  $I_j$  we have  $r$  stencils  $\{S_{j+k}\}_{k=0}^{r-1} = \{(x_{j+k-r+\frac{1}{2}}, x_{j+k-r+\frac{3}{2}}, \dots, x_{j+k+\frac{1}{2}})\}_{k=0}^{r-1}$  which all include two end points  $x_{j-\frac{1}{2}}$  and  $x_{j+\frac{1}{2}}$  of the  $j$ -th cell  $I_j$ . We also have  $r$  interpolating polynomials  $\{\frac{d}{dx}p_{j+k}(x)\}_{k=0}^{r-1}$  on the corresponding stencils  $\{S_{j+k}\}_{k=0}^{r-1}$  from previous subsection. The main idea of the cell-average version of ENO is to choose the “smoothest” one from these  $r$  interpolating polynomials. For Weighted ENO, instead of choosing one, we use all  $r$  interpolating polynomials and compute a convex combination of them to obtain the polynomial  $R_j(x, \bar{u})$  as follows

$$R_j(x, \bar{u}) = \sum_{k=0}^{r-1} \frac{\alpha_k^j}{\sum_{i=0}^{r-1} \alpha_i^j} \frac{d}{dx}p_{j+k}(x), \quad (3.6)$$

where the weights  $\alpha_k^j > 0$  ( $k = 0, 1, 2, \dots, r-1$ ). Obviously  $R_j(x, \bar{u}) = u(x, t) + O(h^r)$  in the smooth regions of  $u(x, t)$  which is the purpose of (3.1a). Note that for any  $k = 0, 1, \dots, r-1$ ,  $p_{j+k}(x_{j-\frac{1}{2}}) = W(x_{j-\frac{1}{2}})$  and  $p_{j+k}(x_{j+\frac{1}{2}}) = W(x_{j+\frac{1}{2}})$ , hence we achieve the purpose of (3.2)

$$\begin{aligned} \frac{1}{h} \int_{I_j} R_j(x, \bar{u}) dx &= \frac{1}{h} \sum_{k=0}^{r-1} \frac{\alpha_k^j}{\sum_{i=0}^{r-1} \alpha_i^j} (p_{j+k}(x_{j+\frac{1}{2}}) - p_{j+k}(x_{j-\frac{1}{2}})) \\ &= \frac{1}{h} \{W(x_{j+\frac{1}{2}}) - W(x_{j-\frac{1}{2}})\} \sum_{k=0}^{r-1} \frac{\alpha_k^j}{\sum_{i=0}^{r-1} \alpha_i^j} = \bar{u}_j. \end{aligned} \quad (3.7)$$

Note that no matter how we define  $\{\alpha_k^j\}_{k=0}^{r-1}$ ,  $R_j(x, \bar{u})$  satisfies the purposes of (3.1a) and (3.2).

Now we define  $\{\alpha_k^j\}_{k=0}^{r-1}$  to achieve the “ENO property”. Here we specify the “ENO property” of  $R_j(x, \bar{u})$  in the sense of corresponding  $\{\alpha_k^j\}_{k=0}^{r-1}$ .

**Definition 1:** The  $R_j(x, \bar{u})$  has the “ENO property” if the corresponding  $\{\alpha_k^j\}_{k=0}^{r-1}$  satisfy that

(i) If the  $(j+k)$ -th stencil  $S_{j+k}$  is in a smooth region of the solution  $u(x, t)$ , the  $\alpha_k^j$  satisfy

$$\frac{\alpha_k^j}{\sum_{l=0}^{r-1} \alpha_l^j} = O(1). \quad (3.8a)$$

(ii) If the  $(j+k)$ -th stencil  $S_{j+k}$  is in a discontinuous region of the solution  $u(x, t)$ , the  $\alpha_k^j$  satisfy

$$\frac{\alpha_k^j}{\sum_{l=0}^{r-1} \alpha_l^j} \leq \max(O(\epsilon^r), O(h^r)), \quad (3.8b)$$

where in this paper we choose  $\epsilon = 10^{-4}$ .

Note that for the  $j$ -th cell  $I_j$ , if  $\{\alpha_k^j\}_{k=0}^{r-1}$  satisfies the “ENO property” (3.8), the  $R_j(x, \bar{u}) = \sum_{k=0}^{r-1} \frac{\alpha_k^j}{\sum_{l=0}^{r-1} \alpha_l^j} \frac{d}{dx} p_{j+k}(x)$  will be a convex combination of the

interpolating polynomials on the smooth stencils (3.8a), and the interpolating polynomials on the discontinuous stencils have essentially no contribution to  $P_j(x)$  (3.8b).

Now let us define  $\{\alpha_k^j\}_{k=0}^{r-1}$ ,

$$\alpha_k^j = C_k^j / (\epsilon + IS_{j+k}^2)^r, \quad (3.9)$$

where  $C_k^j = O(1)$  and  $C_k^j$  will be defined later for improvement of accuracy. Note that because  $IS_{j+k}$  could be zero and  $1/x$  is too sensitive as  $x$  is near zero, we add a small number  $\epsilon$  in the denominator. Also note that if  $(j+k)$ -th stencil  $S_{j+k}$  is in the smooth regions of  $u(x, t)$

$$\frac{\alpha_k^j}{\sum_{l=0}^{r-1} \alpha_l^j} = O(1),$$

and if  $(j+k)$ -th stencil  $S_{j+k}$  is in the discontinuous regions of  $u(x, t)$

$$\frac{\alpha_k^j}{\sum_{l=0}^{r-1} \alpha_l^j} \leq \max(O(\epsilon^r), O(h^{2r})),$$

hence these  $\{\alpha_k^j\}_{k=0}^{r-1}$  (3.9) satisfy the “ENO property” (3.8). Here we assume there is at least one of stencils  $\{S_{j+k}\}_{k=0}^{r-1}$  in smooth regions of  $u(x, t)$ .

Here no matter how we define the constants  $\{C_k^j\}_{k=0}^{r-1}$ , we have achieved the purposes of (3.1a), (3.2) and the “ENO property” (3.8). However we can specify  $\{C_k^j\}_{k=0}^{r-1}$  for (3.1b) which will lead out one order improvement in accuracy in section §3.4, our last purpose of the reconstruction.

For analysis we assume that

$$u(x, t) \in C^{r+1}, \quad (3.10)$$

in  $[x_{j-r+\frac{1}{2}}, x_{j+r+\frac{1}{2}}]$ .

For each  $\frac{d}{dx}p_{j+k}(x)$  which approximates  $u(x, t)$  in  $I_j$ , we express its truncation error as

$$\begin{aligned} e_{j+k}(x) &= u(x, t) - \frac{d}{dx}p_{j+k}(x) \\ &= W'(x) - \frac{d}{dx}p_{j+k}(x) \\ &= \frac{d}{dx}\{W[x, x_{j+k-r+\frac{1}{2}}, \dots, x_{j+k+\frac{1}{2}}] \cdot \prod_{l=0}^r (x - x_{j+k-l+\frac{1}{2}})\} \\ &= \frac{d}{dx}W[x, x_{j+k-r+\frac{1}{2}}, \dots, x_{j+k+\frac{1}{2}}] \cdot \prod_{l=0}^r (x - x_{j+k-l+\frac{1}{2}}) \\ &\quad + W[x, x_{j+k-r+\frac{1}{2}}, \dots, x_{j+k+\frac{1}{2}}] \cdot \sum_{s=0}^r \left\{ \prod_{l=0, l \neq s}^r (x - x_{j+k-l+\frac{1}{2}}) \right\} \\ &= W[x, x_{j+k-r+\frac{1}{2}}, \dots, x_{j+k+\frac{1}{2}}] \cdot a_k^j(x) + O(h^{r+1}), \end{aligned} \quad (3.11a)$$

where  $a_k^j(x) = \sum_{s=0}^r \left\{ \prod_{l=0, l \neq s}^r (x - x_{j+k-l+\frac{1}{2}}) \right\}$ .

We express the truncation error for  $R_j(x, \bar{u})$

$$\begin{aligned} E_j(x) &= u(x, t_n) - R_j(x, \bar{u}) = W'(x) - R_j(x, \bar{u}) \\ &= \sum_{k=0}^{r-1} \frac{\alpha_k^j}{\sum_{i=0}^{r-1} \alpha_i^j} (W'(x) - \frac{d}{dx}p_{j+k}(x)) = \sum_{k=0}^{r-1} \frac{\alpha_k^j}{\sum_{i=0}^{r-1} \alpha_i^j} e_{j+k}(x). \end{aligned}$$

Because of the assumption (3.10),  $\forall k_1, k_2 = 0, 1, \dots, r-1$ ,

$$\begin{aligned} |IS_{j+k_1}| &\leq O(h) \\ |IS_{j+k_1} - IS_{j+k_2}| &\leq O(h) \\ |\alpha_{k_1}^j - \alpha_{k_2}^j| &\leq O(h^2) \\ |W[x, x_{j+k_1-r+\frac{1}{2}}, \dots, x_{j+k_1+\frac{1}{2}}] - W[x, x_{j+k_2-r+\frac{1}{2}}, \dots, x_{j+k_2+\frac{1}{2}}]| &\leq O(h). \end{aligned} \quad (3.11b)$$

We have, from (3.11a) and (3.11b),

$$\begin{aligned}
E_j(x) &= \sum_{k=0}^{r-1} \frac{\alpha_k^j}{\sum_{i=0}^{r-1} \alpha_i^j} e_{j+k}(x) \\
&= \sum_{k=0}^{r-1} \frac{\alpha_k^j}{\sum_{i=0}^{r-1} \alpha_i^j} W[x, x_{j+k-r+\frac{1}{2}}, \dots, x_{j+k+\frac{1}{2}}] \cdot a_k^j(x) + O(h^{r+1}) \\
&= \left\{ \sum_{k=0}^{r-1} \frac{C_k^j}{\sum_{i=0}^{r-1} C_i^j} a_k^j(x) \right\} \cdot W[x, x_{j-r+\frac{1}{2}}, \dots, x_{j+\frac{1}{2}}] + O(h^{r+1}).
\end{aligned} \tag{3.11c}$$

The idea is that for any given point  $x_j^* \in [x_{j-\frac{1}{2}}, x_{j+\frac{1}{2}}]$ , we define  $C_k^j$  to make the first term in (3.11c) equal to zero and we obtain

$$E_j(x_j^*) = O(h^{r+1}).$$

Of course the  $C_k^j$  depend on  $x_j^*$ . For  $x_j^* \in [x_{j-\frac{1}{2}}, x_{j+\frac{1}{2}}]$ , we denote  $\eta_p$  be the number of positive terms in  $\{a_k^j(x_j^*)\}_{k=0}^{r-1}$  and  $\eta_n$  be the number of negative terms in  $\{a_k^j(x_j^*)\}_{k=0}^{r-1}$ , then we define

$$C_k^j = \begin{cases} 1 & \text{if } a_k^j(x_j^*) = 0, \\ \frac{h^r}{\eta_p |a_k^j(x_j^*)|} & \text{if } a_k^j(x_j^*) > 0, \\ \frac{h^r}{\eta_n |a_k^j(x_j^*)|} & \text{if } a_k^j(x_j^*) < 0. \end{cases} \tag{3.12}$$

Here, obviously the  $C_k^j$  are independent of grid size  $h$ . Now

$$\begin{aligned}
E_j(x_j^*) &= \left\{ \sum_{k=0}^{r-1} \frac{C_k^j}{\sum_{i=0}^{r-1} C_i^j} a_k^j(x_j^*) \right\} W[x, x_{j-r+\frac{1}{2}}, \dots, x_{j+\frac{1}{2}}] + O(h^{r+1}) \\
&= \left\{ \sum_{a_k^j(x_j^*) > 0} \frac{\frac{1}{\eta_p}}{\sum_{i=0}^{r-1} C_i^j} - \sum_{a_k^j(x_j^*) < 0} \frac{\frac{1}{\eta_n}}{\sum_{i=0}^{r-1} C_i^j} \right\} W[x, x_{j-r+\frac{1}{2}}, \dots, x_{j+\frac{1}{2}}] + O(h^{r+1}) \\
&= 0 + O(h^{r+1}) \\
&= O(h^{r+1}).
\end{aligned} \tag{3.13}$$

*Remark 2:* We have to have  $\eta_p \geq 1$  and  $\eta_n \geq 1$  to guarantee (3.13).

Thus we obtain that, for any given point  $x_j^*$  and any other point  $x \in [x_{j-\frac{1}{2}}, x_{j+\frac{1}{2}}]$ , defining  $C_k^j$  by (3.12) gives us

$$E_j(x) = O(h^r), \quad (3.14a)$$

and

$$E_j(x_j^*) = O(h^{r+1}). \quad (3.14b)$$

Up to now, we have achieved all purposes of reconstruction (3.1a), (3.1b), (3.2) and (3.8).

### 3.4 One Order Improvement in Accuracy from (3.1b)

In this subsection, we shall see how (3.1b) or (3.14b) gives us one order of improvement in accuracy by choosing  $x_j^*$  properly in each cell. Let us consider the numerical spatial approximation (2.7b)

$$L_j(\bar{u}) = -\frac{1}{h} [ \tilde{h}(R_j(x_{j+\frac{1}{2}}, \bar{u}), R_{j+1}(x_{j+\frac{1}{2}}, \bar{u})) - \tilde{h}(R_{j-1}(x_{j-\frac{1}{2}}, \bar{u}), R_j(x_{j-\frac{1}{2}}, \bar{u})) ].$$

According to remark 1, in general, we only can achieve  $L_j(\bar{u}) = \Phi_j(u) + O(h^r)$ . Here we shall give the analysis of how (3.1b) lead to one order of improvement in accuracy i.e.

$$L_j(\bar{u}) = \Phi_j(u) + O(h^{r+1}),$$

in most cells.

We notice that  $\tilde{h}(a, b)$  ( see (2.4), (2.5) and (2.6) ) is equal to either  $f(a)$  or  $f(b)$  away from sonic points. Let us consider three cells in a smooth region, say cells  $I_{j-1}$ ,  $I_j$  and  $I_{j+1}$ , which are away from sonic points.

If  $f'(R(x, \bar{u})) > 0$  in the cells. We have

$$L_j(\bar{u}) = -\frac{1}{h} [f(R_j(x_{j+\frac{1}{2}}, \bar{u})) - f(R_{j-1}(x_{j-\frac{1}{2}}, \bar{u}))].$$

Now if in the  $j$ -th cell we chose  $x_j^*$  to be the right end point of the cell i.e.  $x_j^* = x_{j+\frac{1}{2}}$  to define corresponding  $C_k^j$  and in  $(j-1)$ -th cell we also chose  $x_{j-1}^*$  to be the right end point of the cell i.e.  $x_{j-1}^* = x_{j-\frac{1}{2}}$  to define corresponding  $C_k^{j-1}$ , then by (3.14b) we obtain that

$$R_j(x_{j+\frac{1}{2}}) - u(x_{j+\frac{1}{2}}, t_n) = E_j(x_{j+\frac{1}{2}}) = O(h^{r+1}),$$

$$R_{j-1}(x_{j-\frac{1}{2}}) - u(x_{j-\frac{1}{2}}, t_n) = E_j(x_{j-\frac{1}{2}}) = O(h^{r+1}).$$

Thus

$$L_j(\bar{u}) = -\frac{1}{h}[f(u(x_{j+\frac{1}{2}}, t_n)) - f(u(x_{j-\frac{1}{2}}, t_n))] + O(h^{r+1}).$$

If  $f'(R(x, \bar{u})) < 0$  in the cells. We have

$$L_j(\bar{u}) = -\frac{1}{h}[f(R_{j+1}(x_{j+\frac{1}{2}}, \bar{u})) - f(R_j(x_{j-\frac{1}{2}}, \bar{u}))].$$

Now if in the  $j$ -th cell we chose  $x_j^*$  to be the left end point of the cell i.e.  $x_j^* = x_{j-\frac{1}{2}}$  to define corresponding  $C_k^j$  and in  $(j+1)$ -th cell we also chose  $x_{j+1}^*$  to be the left end point of the cell i.e.  $x_{j+1}^* = x_{j+\frac{1}{2}}$  to define corresponding  $C_k^{j+1}$ , then by (3.14b) we obtain that

$$R_{j+1}(x_{j+\frac{1}{2}}) - u(x_{j+\frac{1}{2}}, t_n) = E_j(x_{j+\frac{1}{2}}) = O(h^{r+1}),$$

$$R_j(x_{j-\frac{1}{2}}) - u(x_{j-\frac{1}{2}}, t_n) = E_j(x_{j-\frac{1}{2}}) = O(h^{r+1}).$$

Thus

$$L_j(\bar{u}) = -\frac{1}{h}[f(u(x_{j+\frac{1}{2}}, t_n)) - f(u(x_{j-\frac{1}{2}}, t_n))] + O(h^{r+1}).$$

Hence in the smooth regions of the solution and away from sonic points, the numerical spatial operators  $\{L_j(\bar{u})\}$  approximate the spatial operators  $\{\Phi_j(u)\}$  in the order of  $O(h^{r+1})$  if we choose  $x_j^*$  properly in each cell.

We specify  $x_j^*$  in each cell in the following way:

First we compute  $f'(\bar{u}_j)$ . Then

(i) if  $f'(\bar{u}_j) > 0$  we chose  $x_j^*$  to be the right end point of  $j$ -th cell i.e.  $x_j^* = x_{j+\frac{1}{2}}$ ,

(ii) if  $f'(\bar{u}_j) < 0$  we chose  $x_j^*$  to be the left end point of  $j$ -th cell i.e.  $x_j^* = x_{j-\frac{1}{2}}$ ,

(iii) if  $f'(\bar{u}_j) = 0$  we chose  $x_j^*$  to be either the right end point or the left end point of  $j$ -th cell i.e.  $x_j^* = x_{j+\frac{1}{2}}$  or  $x_j^* = x_{j-\frac{1}{2}}$ .

Now if the  $j$ -th cell is in the smooth regions of the solution and away from sonic points which means  $f'(\bar{u}_j) \neq 0$ , then in general  $f'(R(x, \bar{u})) \cdot f'(\bar{u}_j) > 0$  around the  $j$ -th cell  $I_j$ , hence according to the above analysis

$$L_j(\bar{u}) = \Phi_j(u) + O(h^{r+1}). \quad (3.15)$$



Because sonic points are isolated, in general, we obtain (3.15) in most of the cells and obtain

$$L_j(\bar{u}) = \Phi_j(u) + O(h^r)$$

in a bounded, in fact small, number of cells near which there are sonic points as  $h$  decrease to zero.

*Remark 3:* We have achieved one order improvement in accuracy. For  $r = 2$  and  $r = 3$ , the cost of computing between the Weighted ENO schemes and the corresponding standard ENO schemes ( with the same order ) are comparable on sequential computers. But on parallel computers the former schemes are less expensive than the latter ones because the latter ones need more highly costing data transportation among cells not within short distance.

### 3.5 The Schemes when $r = 2$

The purpose of following two subsections §3.5 and §3.6 is to spell out the details of the general schemes for two specific values of  $r$ , perhaps to help people to implement the schemes.

In this subsection, we consider our schemes when  $r = 2$ . In this case we only use linear interpolation to achieve the “ENO property” and 3rd order accuracy ( in numerical experiments, we achieve 4th order accuracy ) with conservation form.

Here we only give the reconstruction procedure for  $r = 2$ . Let us construct the solution in each cell  $I_j$ . We have two stencils  $S_j = (x_{j-\frac{3}{2}}, x_{j-\frac{1}{2}}, x_{j+\frac{1}{2}})$  and  $S_{j+1} = (x_{j-\frac{1}{2}}, x_{j+\frac{1}{2}}, x_{j+\frac{3}{2}})$  corresponding to  $I_j = [x_{j-\frac{1}{2}}, x_{j+\frac{1}{2}}]$ . On these two stencils, we obtain linear interpolations

$$\frac{d}{dx}p_j(x) = \bar{u}_j + \frac{\bar{u}_j - \bar{u}_{j-1}}{h}(x - x_j)$$

and

$$\frac{d}{dx}p_{j+1}(x) = \bar{u}_j + \frac{\bar{u}_{j+1} - \bar{u}_j}{h}(x - x_j),$$

and two indicators of smoothness  $IS_j = |\bar{u}_j - \bar{u}_{j-1}|$  and  $IS_{j+1} = |\bar{u}_{j+1} - \bar{u}_j|$ . The reconstructed solution  $R_j(x, \bar{u})$  will be a convex combination of  $\frac{d}{dx}p_j(x)$  and  $\frac{d}{dx}p_{j+1}(x)$  i.e.

$$R_j(x, \bar{u}) = \frac{\alpha_0^j}{\alpha_0^j + \alpha_1^j} \frac{d}{dx}p_j(x) + \frac{\alpha_1^j}{\alpha_0^j + \alpha_1^j} \frac{d}{dx}p_{j+1}(x), \quad (3.16)$$

where  $\alpha_0^j = C_0^j/(\epsilon + IS_j^2)^2$ ,  $\alpha_1^j = C_1^j/(\epsilon + IS_{j+1}^2)^2$  and  $\epsilon = 10^{-4}$ . We shall specify  $C_0^j$  and  $C_1^j$  in the following two cases.

Case 1: If  $f'(\bar{u}_j) > 0$ , we choose  $x_j^* = x_{j+\frac{1}{2}}$ . We compute  $a_0^j(x_{j+\frac{1}{2}}) = 2h^2$  and  $a_1^j(x_{j+\frac{1}{2}}) = -h^2$ , and obtain  $\eta_p = 1$  and  $\eta_n = 1$ , hence  $C_0^j = 1/2$  and  $C_1^j = 1$ . Thus

$$\begin{aligned}\alpha_0^j &= \frac{1}{2(\epsilon + IS_j^2)^2} \\ \alpha_1^j &= \frac{1}{(\epsilon + IS_{j+1}^2)^2}\end{aligned}\tag{3.17a}$$

in (3.16).

Case 2: If  $f'(\bar{u}_j) \leq 0$ , we choose  $x_j^* = x_{j-\frac{1}{2}}$ . We compute  $a_0^j(x_{j-\frac{1}{2}}) = -h^2$  and  $a_1^j(x_{j-\frac{1}{2}}) = 2h^2$ , and obtain  $\eta_p = 1$  and  $\eta_n = 1$ , hence  $C_0^j = 1$  and  $C_1^j = 1/2$ . Thus

$$\begin{aligned}\alpha_0^j &= \frac{1}{(\epsilon + IS_j^2)^2} \\ \alpha_1^j &= \frac{1}{2(\epsilon + IS_{j+1}^2)^2}\end{aligned}\tag{3.17b}$$

in (3.16).

### 3.6 The Schemes when $r = 3$

In this subsection, we consider our schemes when  $r = 3$ . In this case we only use quadratic interpolation to achieve the ‘‘ENO property’’ and 4th order accuracy ( in numerical experiments, we achieve 5th order accuracy ) with conservation form.

Here we only give out the reconstruction procedure for  $r = 3$ . Let us construct the solution in each cell  $I_j$ . We have three stencils  $S_j = (x_{j-\frac{5}{2}}, x_{j-\frac{3}{2}}, x_{j-\frac{1}{2}}, x_{j+\frac{1}{2}})$ ,  $S_{j+1} = (x_{j-\frac{3}{2}}, x_{j-\frac{1}{2}}, x_{j+\frac{1}{2}}, x_{j+\frac{3}{2}})$ , and  $S_{j+2} = (x_{j-\frac{1}{2}}, x_{j+\frac{1}{2}}, x_{j+\frac{3}{2}}, x_{j+\frac{5}{2}})$  corresponding to  $I_j = [x_{j-\frac{1}{2}}, x_{j+\frac{1}{2}}]$ . On these three stencils, we obtain quadratic interpolations

$$\begin{aligned}\frac{d}{dx}p_j(x) &= \frac{\bar{u}_j - 2\bar{u}_{j-1} + \bar{u}_{j-2}}{2h^2}(x - x_{j-1})^2 + \frac{\bar{u}_j - \bar{u}_{j-2}}{2h}(x - x_{j-1}) + \\ &\quad \frac{\bar{u}_{j-1} - \bar{u}_{j-2}}{24}, \\ \frac{d}{dx}p_{j+1}(x) &= \frac{\bar{u}_{j+1} - 2\bar{u}_j + \bar{u}_{j-1}}{2h^2}(x - x_j)^2 + \frac{\bar{u}_{j+1} - \bar{u}_{j-1}}{2h}(x - x_j) + \\ &\quad \frac{\bar{u}_j - \bar{u}_{j-1}}{24},\end{aligned}$$

and

$$\frac{d}{dx}p_{j+2}(x) = \frac{\bar{u}_{j+2}-2\bar{u}_{j+1}+\bar{u}_j}{2h^2}(x-x_{j+1})^2 + \frac{\bar{u}_{j+2}-\bar{u}_j}{2h}(x-x_{j+1}) + \frac{\bar{u}_{j+1}-\bar{u}_{j+2}-2\bar{u}_{j+1}+\bar{u}_j}{24},$$

and three indicators of smoothness  $IS_j = (|\bar{u}_{j-1} - \bar{u}_{j-2}| + |\bar{u}_j - \bar{u}_{j-1}|)/2 + |\bar{u}_j - 2\bar{u}_{j-1} + \bar{u}_{j-2}|$ ,  $IS_{j+1} = (|\bar{u}_j - \bar{u}_{j-1}| + |\bar{u}_{j+1} - \bar{u}_j|)/2 + |\bar{u}_{j+1} - 2\bar{u}_j + \bar{u}_{j-1}|$  and  $IS_{j+2} = (|\bar{u}_{j+1} - \bar{u}_j| + |\bar{u}_{j+2} - \bar{u}_{j+1}|)/2 + |\bar{u}_{j+2} - 2\bar{u}_{j+1} + \bar{u}_j|$ . The reconstructed solution  $R_j(x, \bar{u})$  will be a convex combination of  $\frac{d}{dx}p_j(x)$ ,  $\frac{d}{dx}p_{j+1}(x)$  and  $\frac{d}{dx}p_{j+2}(x)$  i.e.

$$R_j(x, \bar{u}) = \frac{\alpha_0^j}{\alpha_0^j + \alpha_1^j + \alpha_2^j} \frac{d}{dx}p_j(x) + \frac{\alpha_1^j}{\alpha_0^j + \alpha_1^j + \alpha_2^j} \frac{d}{dx}p_{j+1}(x) + \frac{\alpha_2^j}{\alpha_0^j + \alpha_1^j + \alpha_2^j} \frac{d}{dx}p_{j+2}(x), \quad (3.18)$$

where  $\alpha_0^j = C_0^j/(\epsilon + IS_j^2)^3$ ,  $\alpha_1^j = C_1^j/(\epsilon + IS_{j+1}^2)^3$ ,  $\alpha_2^j = C_2^j/(\epsilon + IS_{j+2}^2)^3$  and  $\epsilon = 10^{-4}$ . We shall specify  $C_0^j$ ,  $C_1^j$  and  $C_2^j$  in the following two cases.

Case 1: If  $f'(\bar{u}_j) > 0$ , we choose  $x_j^* = x_{j+\frac{1}{2}}$ . We compute  $a_0^j(x_{j+\frac{1}{2}}) = 6h^3$ ,  $a_1^j(x_{j+\frac{1}{2}}) = -2h^3$  and  $a_2^j(x_{j+\frac{1}{2}}) = 2h^3$ , and obtain  $\eta_p = 2$  and  $\eta_n = 1$ , hence  $C_0^j = 1/12$ ,  $C_1^j = 1/2$  and  $C_2^j = 1/4$ . Thus

$$\begin{aligned} \alpha_0^j &= \frac{1}{12(\epsilon + IS_j^2)^3} \\ \alpha_1^j &= \frac{1}{2(\epsilon + IS_{j+1}^2)^3} \\ \alpha_2^j &= \frac{1}{4(\epsilon + IS_{j+2}^2)^3} \end{aligned} \quad (3.19a)$$

in (3.18).

Case 2: If  $f'(\bar{u}_j) \leq 0$ , we choose  $x_j^* = x_{j-\frac{1}{2}}$ . We compute  $a_0^j(x_{j-\frac{1}{2}}) = -2h^3$ ,  $a_1^j(x_{j-\frac{1}{2}}) = 2h^3$ , and  $a_2^j(x_{j-\frac{1}{2}}) = -6h^3$  and obtain  $\eta_p = 1$  and  $\eta_n = 2$ , hence  $C_0^j = 1/4$ ,  $C_1^j = 1/2$  and  $C_2^j = 1/12$ . Thus

$$\begin{aligned} \alpha_0^j &= \frac{1}{4(\epsilon + IS_j^2)^3} \\ \alpha_1^j &= \frac{1}{2(\epsilon + IS_{j+1}^2)^3} \\ \alpha_2^j &= \frac{1}{12(\epsilon + IS_{j+2}^2)^3} \end{aligned} \quad (3.19b)$$

in (3.18).

## 4 The Numerical Experiments

### 4.1 Scalar Conservation Laws

In this subsection we use some model problems to numerically test our schemes. We use the Roe flux with entropy fix as numerical flux and choose  $r = 2$  which means we use a linear polynomial to reconstruct the solution, and  $r = 3$  which means we use a quadratic polynomial to reconstruct the solution, and we expect to achieve 3rd and 4th order accuracy respectively ( at least away from sonic points ) according to our analysis in the previous section.

*Example 1.* We solve the model equation

$$\begin{aligned} u_t + u_x &= 0 & -1 \leq x \leq 1 \\ u(x, 0) &= u_0(x) & u_0(x) \text{ periodic with period } 2. \end{aligned} \quad (4.1)$$

Five different initial data  $u_0(x)$  are used. The first one is  $u_0(x) = \sin(\pi x)$  and we list the errors at time  $t=1$  in Table 1. The second one is  $u_0(x) = \sin^4(\pi x)$  and we list the errors at time  $t=1$  in Table 2.

**TABLE 1** (  $\tau/h=0.6$ ,  $t=1$  )

$l$	$L_1$ error	$L_1$ order	$L_\infty$ error	$L_\infty$ order
$r = 2$				
80	2.81D-03		1.22D-02	
160	1.99D-04	3.82	1.11D-03	3.46
320	1.06D-05	4.23	4.27D-05	4.70
640	5.09D-07	4.38	1.55D-06	4.78
$r = 3$				
80	1.41D-05		6.34D-05	
160	3.01D-07	5.55	1.71D-06	5.21
320	8.21D-09	5.20	2.12D-08	6.33
640	1.89D-10	5.44	4.54D-10	5.55

TABLE 2 (  $\tau/h=0.6, t=1$  )

$l$	$L_1$ error	$L_1$ order	$L_\infty$ error	$L_\infty$ order
$r = 2$				
80	1.78D-02		7.24D-02	
160	3.12D-03	2.51	1.87D-02	1.95
320	2.47D-04	3.66	2.04D-03	3.20
640	1.40D-05	4.14	9.14D-05	4.48
$r = 3$				
80	1.48D-03		4.84D-03	
160	5.44D-05	4.77	2.24D-04	4.43
320	1.09D-06	5.64	7.51D-06	4.90
640	1.67D-08	6.03	9.77D-08	6.26

Here and below  $l$  is the total number of cells and the step size  $h = 2/l$  in all scalar examples.

For the first two initial data, we obtain about 4th ( for  $r = 2$  ) and 5th ( for  $r = 3$  ) order of accuracy respectively in the smooth region in both  $L_1$  and  $L_\infty$  norms which is surprisingly better than the 3rd and 4-th order, the theoretical results. We note that standard ENO schemes applied to the example with the second initial data experienced an (easily fixed) loss of accuracy, see [6], [7]. No such degeneracy was found with our present methods.

The third initial function is

$$u_0(x) = \begin{cases} 1 & -\frac{1}{5} \leq x \leq \frac{1}{5}, \\ 0 & \text{otherwise,} \end{cases}$$

the fourth is

$$u_0(x) = \begin{cases} (1 - (\frac{10}{3}x)^2)^{\frac{1}{2}} & -\frac{3}{10} \leq x \leq \frac{3}{10}, \\ 0 & \text{otherwise,} \end{cases}$$

and the fifth is

$$u_0(x) = e^{-300x^2}.$$

We see the good resolution of the solutions in Figures 1-3 which are obtained by our scheme with  $r = 3$ . Linear discontinuities are smeared a bit. We expect to fix this in the future using either the subcell resolution technique of Harten [10] or the artificial compression technique of Yang [11] together with the present technique.

**Figure 1 (  $\tau/h = 0.6$  )**

The solution by WENO at T = 0.5

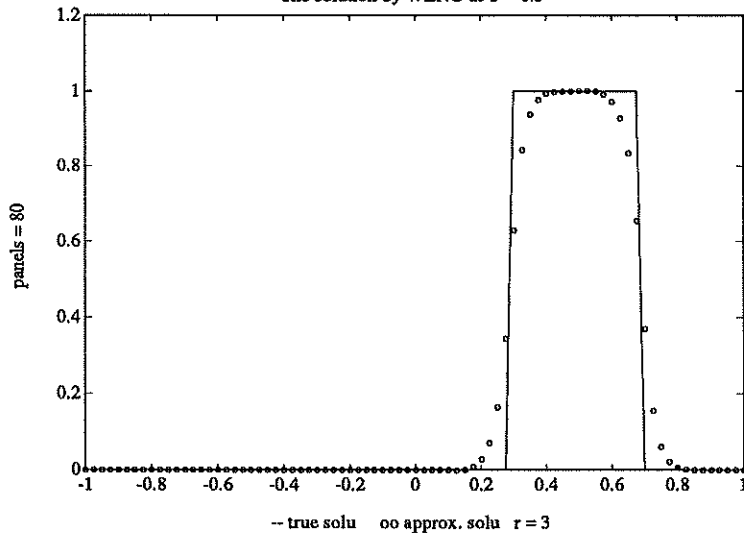


**Figure 2 (  $\tau/h = 0.6$  )**

The solution by WENO at T = 0.5

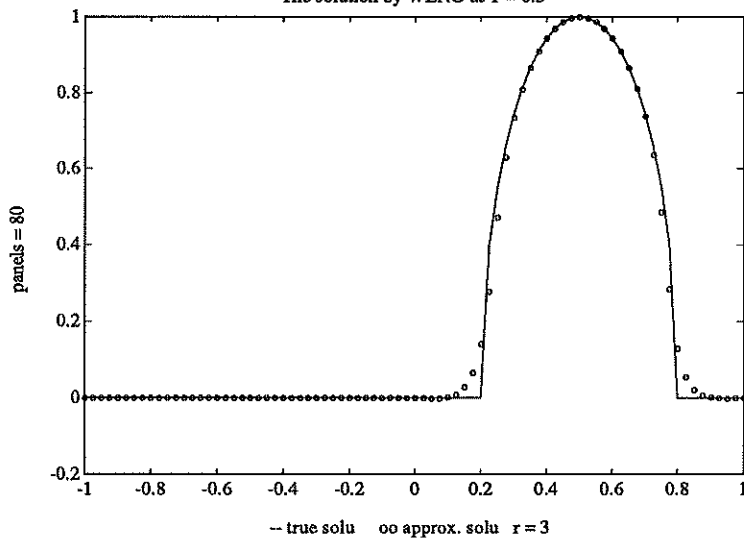
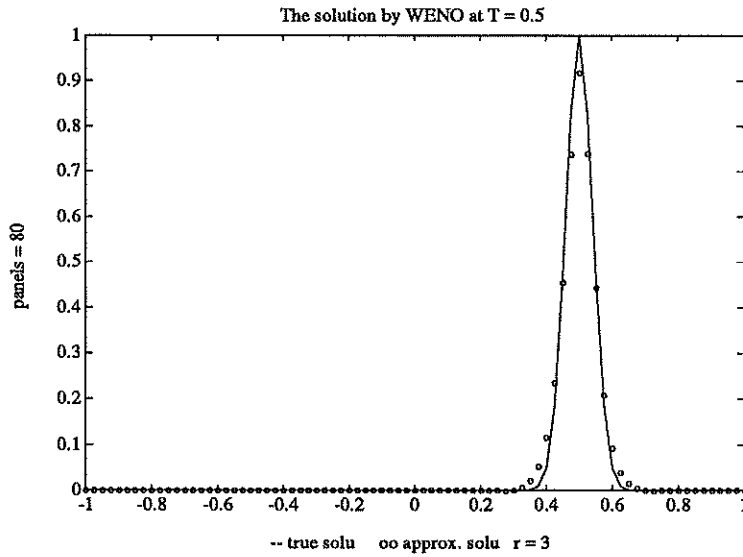


**Figure 3** (  $\tau/h = 0.6$  )



*Example 2.* We solve Burgers' equation with a periodic boundary condition

$$\begin{aligned} u_t + \left(\frac{1}{2}u^2\right)_x &= 0 & -1 \leq x \leq 1 \\ u(x, 0) &= u_0(x) & u_0(x) \text{ periodic with period } 2. \end{aligned} \quad (4.2)$$

For the initial data  $u_0(x) = 1 + \frac{1}{2}\sin(\pi x)$ , the exact solution is smooth up to  $t = \frac{2}{\pi}$ , then it develops a moving shock which interacts with a rarefaction wave.

At  $t = 0.3$  the solution is still smooth. We list the errors in Table 3. Note we also have about 4th ( for  $r = 2$  ) and 5th ( for  $r = 3$  ) order of accuracy respectively both in  $L_1$  and  $L_\infty$  norms.

**TABLE 3** (  $\tau/h=0.6, t=0.3$  )

$l$	$L_1$ error	$L_1$ order	$L_\infty$ error	$L_\infty$ order
$r = 2$				
80	3.47D-04		1.78D-03	
160	2.53D-05	3.78	1.17D-04	3.93
320	1.80D-06	3.81	9.81D-06	3.58
640	1.36D-07	3.73	7.88D-07	3.64
$r = 3$				
80	8.60D-06		8.53D-05	
160	2.62D-07	5.04	1.83D-06	5.55
320	8.94D-09	4.87	7.50D-08	4.61
640	4.87D-10	4.20	3.41D-09	4.46

At  $t = \frac{2}{\pi}$  the shock just begins to form, at  $t = 1.1$  the interaction between the shock and the rarefaction waves is over, and the solution becomes monotone between shocks. In Figures 4-5 which are obtain by our scheme with  $r = 3$  we can see the excellent behavior of the schemes in both cases. The errors at a distance 0.1 away from the shock ( i.e.  $|x - \text{shock location}| \geq 0.1$  ) are listed in Table 4 at  $t = 1.1$ . These errors are of a little larger magnitude than the ones in the smooth case of Table 3 and show about 4th ( for  $r = 2$  ) and 5th ( for  $r = 3$  ) order of accuracy respectively both in  $L_1$  and  $L_\infty$  in the smooth regions 0.1 away from the shock. This shows that the error propagation of the scheme is still very local.

**TABLE 4** (  $\tau/h=0.6, t=1.1$  )

$l$	$L_1$ error	$L_1$ order	$L_\infty$ error	$L_\infty$ order
$r = 2$				
80	1.22D-04		3.44D-03	
160	5.31D-06	4.52	6.79D-05	5.66
320	3.74D-07	3.83	2.62D-06	4.70
$r = 3$				
80	1.86D-05		4.84D-04	
160	8.16D-07	4.51	4.80D-05	3.33
320	1.34D-08	5.93	1.19D-06	5.34



Figure 4 (  $\tau/h = 0.6$  )

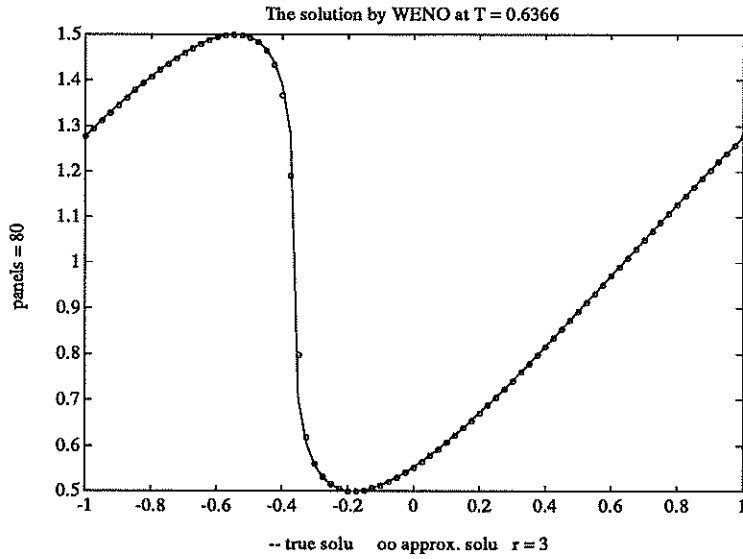
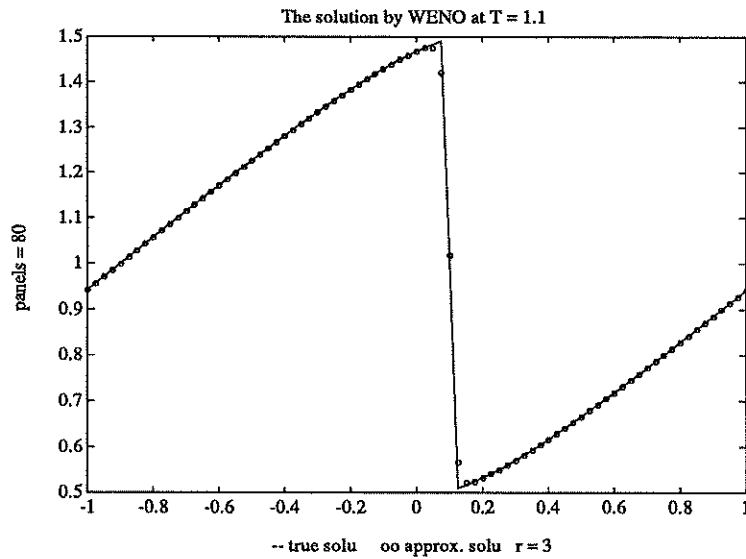


Figure 5 (  $\tau/h = 0.6$  )



*Example 3.* we use two nonconvex fluxes to test the convergence to the physically correct solutions. The true solutions are obtained from the Lax-Friedrichs scheme on a very fine grid. We use our scheme with  $r = 3$  in this example. The first one is a Riemann problem with the flux  $f(u) =$

$\frac{1}{4}(u^2 - 1)(u^2 - 4)$ , and the initial data

$$u_0(x) = \begin{cases} u_l & x < 0 \\ u_r & x > 0. \end{cases}$$

The two cases we test are (i)  $u_l = 2, u_r = -2$ , Figure 6; (ii)  $u_l = -3, u_r = 3$ , Figure 7. For more details concluding this problem see [2]

**Figure 6 (  $\tau/h = 0.3$  )**

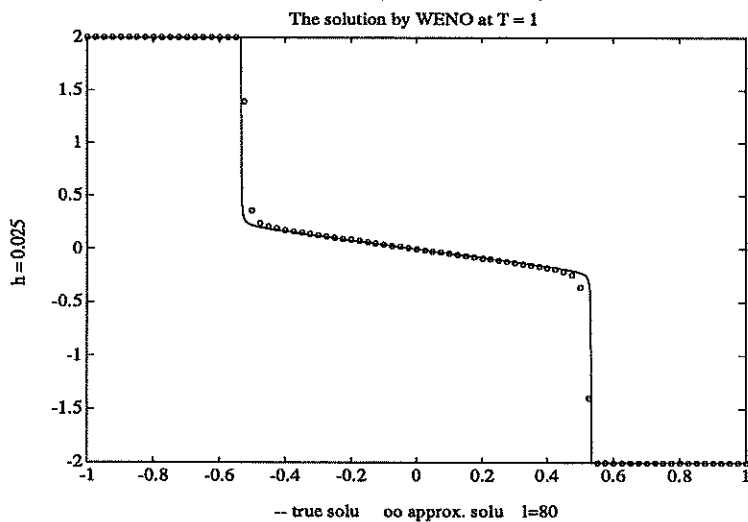
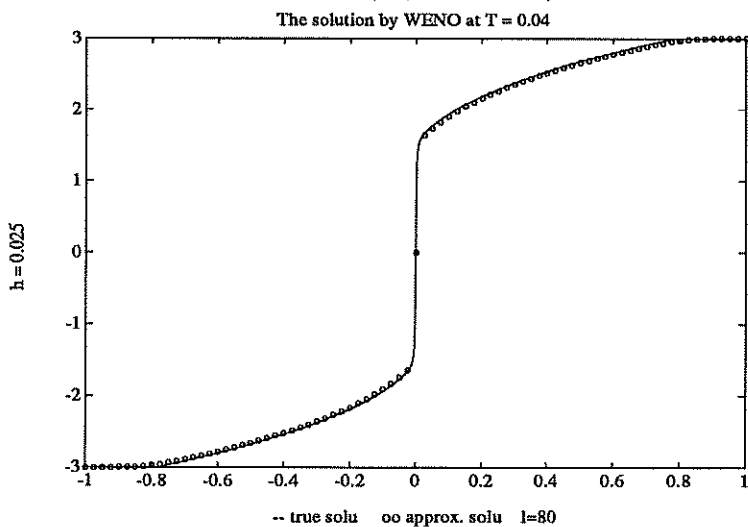
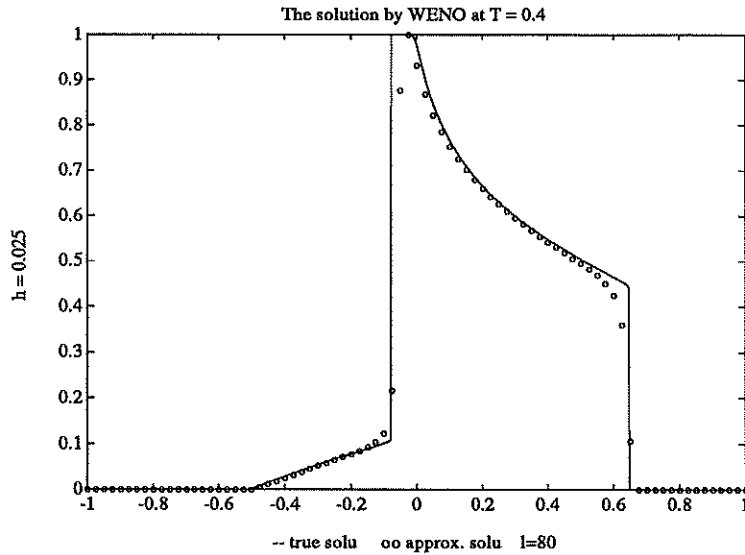


**Figure 7 (  $\tau/h = 0.04$  )**



The second flux is the Buckley-Leverett flux used to model oil recovery [2],  $f(u) = 4u^2/(4u^2 + (1 - u)^2)$ , with initial data  $u = 1$  in  $[-\frac{1}{2}, 0]$  and  $u = 0$  elsewhere. The result is displayed in Figure 8.

Figure 8 (  $\tau/h = 0.4$  )



In this example, we observe convergence with good resolution to the entropy solutions in both cases.

In all the examples that we have illustrated above, we observe that the schemes are of about 4th ( for  $r = 2$  ) and 5th ( for  $r = 3$  ) order of accuracy respectively and convergent with good resolution to the entropy solutions.

## 4.2 Euler Equations of Gas Dynamics

In this subsection we apply our schemes to the Euler equation of gas dynamics for a polytropic gas,

$$\begin{aligned}
 u_t + f(u)_x &= 0 \\
 u &= (\rho, m, E)^T \\
 f(u) &= qu + (0, P, qP)^T \\
 P &= (\gamma - 1)(E - \frac{1}{2}\rho q^2) \\
 m &= \rho q,
 \end{aligned} \tag{4.2}$$

where  $\gamma = 1.4$  in the following computation. For details of the Jacobian, its eigenvalues, eigenvectors, etc., see [2].

*Example 4.* We consider the following Riemann problems:

$$u_0(x) = \begin{cases} u_l & x < 0 \\ u_r & x > 0. \end{cases}$$

Two sets of initial data are used. One is proposed by Sod in [8]:

$$(\rho_l, q_l, P_l) = (1, 0, 1); \quad (\rho_r, q_r, P_r) = (0.125, 0, 0.1).$$

The other is used by Lax [9]:

$$(\rho_l, q_l, P_l) = (0.445, 0.698, 3.528); \quad (\rho_r, q_r, P_r) = (0.5, 0, 0.571).$$

We test our schemes with  $r = 3$  and set  $\epsilon = 10^{-9}$  only in this example. We use the characteristic reconstruction and Roe flux with entropy fix formed by Roe's average as numerical flux. For details see [2]. The results are displayed in Figure 9-10.

**Figure 9a** ( $\tau/h = 0.4, t = 2$ )

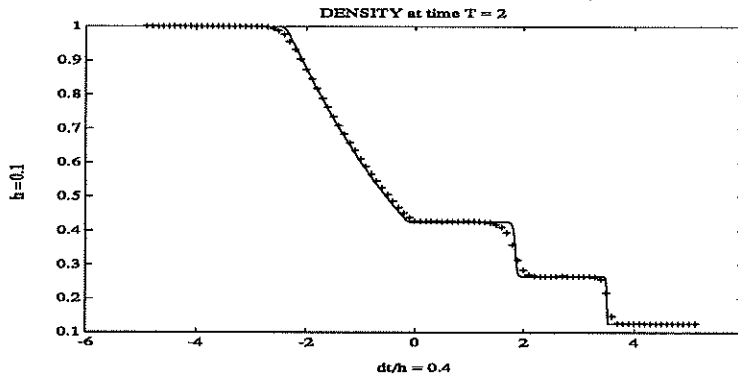


**Figure 9b** ( $\tau/h = 0.4, t = 2$ )

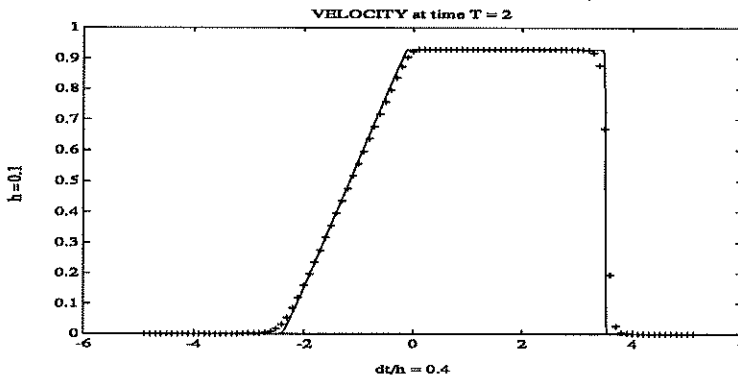


Figure 9c (  $\tau/h = 0.4, t = 2$  )

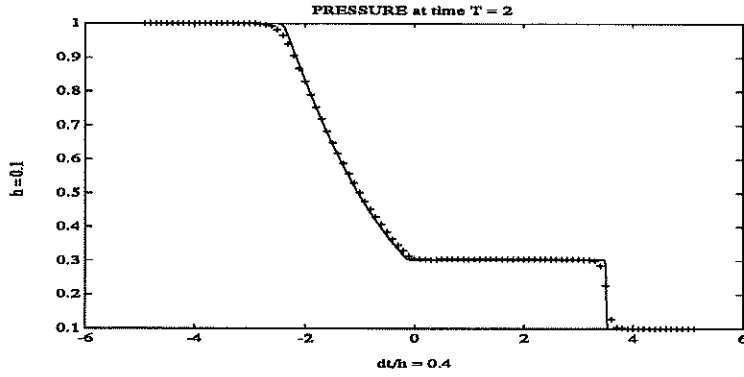


Figure 10a (  $\tau/h = 0.2, t = 1.5$  )

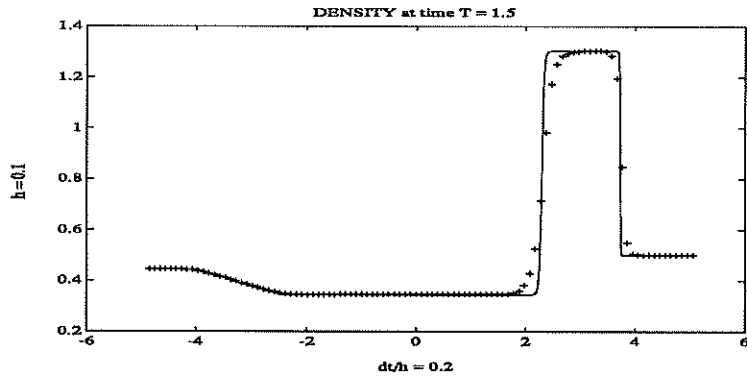


Figure 10b (  $\tau/h = 0.2, t = 1.5$  )

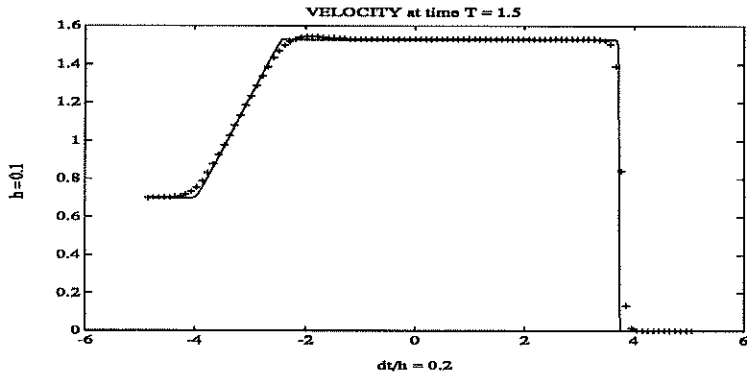
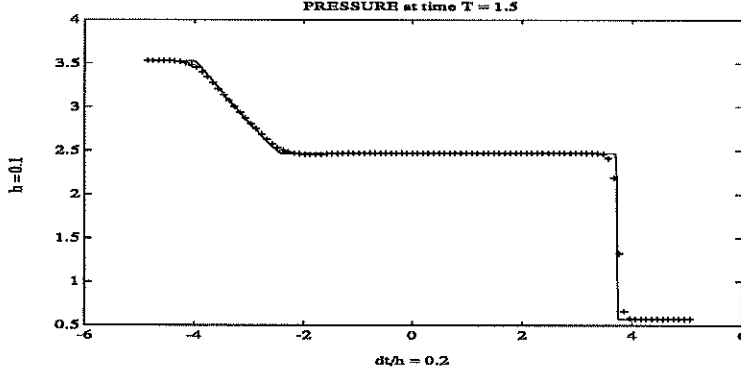


Figure 10c (  $\tau/h = 0.2, t = 1.5$  )



*Example 5.* In this example we shall test the accuracy of our schemes (  $r = 3$  ) for the Euler equation of gas dynamics for a polytropic gas. We choose initial data as  $\rho = 2 + \sin(\pi x)$ ,  $m = 2 + \sin(\pi x)$  and  $E = 2 + \sin(\pi x)$ , and periodic boundary condition. The solution was obtained by applying the schemes to a very fine grid. For time  $t = 1$  when shocks haven't formed, our schemes achieve 5th (  $r = 3$  ) order accuracy in all three components, see Table 5. We can also see the solution for time  $t = 1$  in Figure 11.

TABLE 5 (  $\tau/h=0.6, t=1$  )

$l$	$L_1$ error	$L_1$ order	$L_\infty$ error	$L_\infty$ order
DENSITY				
80	1.16D-04		8.60D-04	
160	2.85D-06	5.35	2.53D-05	5.09
320	5.89D-08	5.60	5.97D-07	5.41
MOMENTUM				
80	1.25D-04		1.13D-03	
160	3.06D-06	5.35	3.22D-05	5.13
320	7.55D-08	5.34	6.44D-07	5.64
ENERGY				
80	1.28D-04		1.20D-03	
160	2.85D-06	5.49	4.04D-05	4.89
320	7.04D-08	5.34	7.74D-07	5.71

Figure 11a (  $\tau/h = 0.6, t = 1$  )

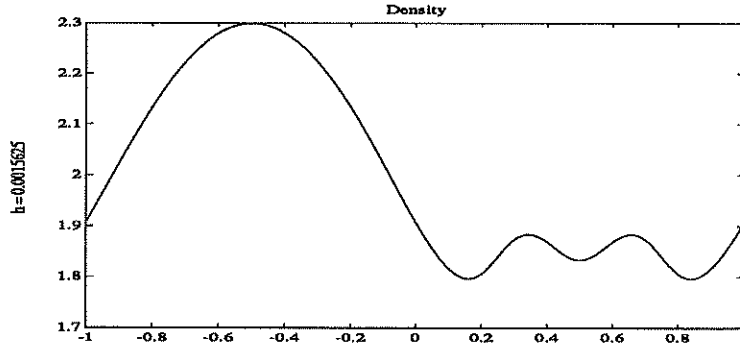


Figure 11b (  $\tau/h = 0.6, t = 1$  )

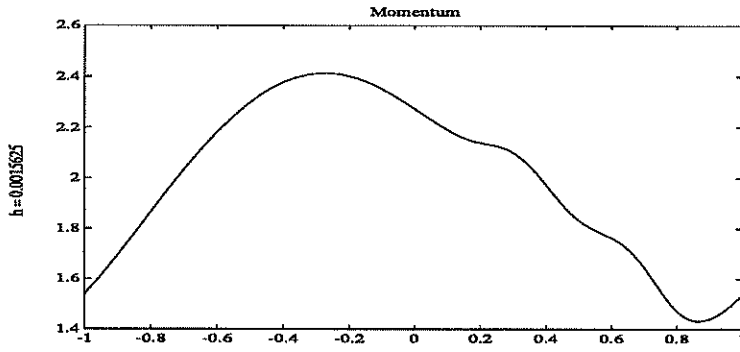
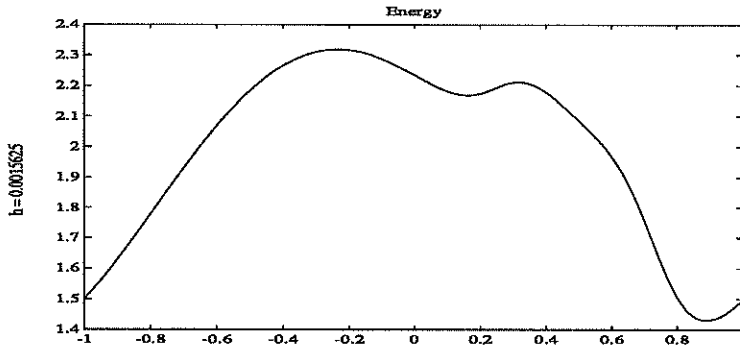


Figure 11c (  $\tau/h = 0.6, t = 1$  )



## References

- [1] A. Harten and S. Osher, "Uniformly High-Order Accurate Non-Oscillatory Schemes I," *SIAM Journal on Numerical Analysis*, V24, pp. 279-309, 1987; also MRC Technical Summary Report No. 2823, May 1985.
- [2] A. Harten, B. Engquist, S. Osher and S. Chakravarthy, "Uniformly High Order Accurate Essentially Non-Oscillatory Schemes III," *Journal of Computational Physics*, V71, pp. 231-303, 1987; also ICASE Report No. 86-22, April 1986.
- [3] C.-W. Shu and S. Osher, "Efficient Implementation of Essentially Non-oscillatory Shock-Capturing Schemes," *Journal of Computational Physics*, V77, 1988, pp. 439-471.
- [4] Chi-Wang Shu, Stanley Osher, "Efficient Implementation of Essentially Non-oscillatory Shock-Capturing Schemes, II," *J. Comput. Phys.*, V83, 1989, pp. 32-78.
- [5] A. Harten and S. Chakravarthy, "Multi-Dimensional ENO Schemes for General Geometries," UCLA CAM report No. 91-16, August 1991.
- [6] A. Rogerson and E. Meiburg, "A Numerical Study of the Convergence Properties of ENO Schemes," *J. Scientific Computing*, V5, No.2, 1990, pp.151-167.
- [7] Chi-Wang Shu, "Numerical Experiments on the Accuracy of ENO and Modified ENO Schemes," *J. Scientific Computing*, V5, No.2, 1990, pp.127-149.
- [8] G. Sod, *J. Comput. Phys.* 27, 1 (1978).
- [9] P. Lax. *Commun. Pure Appl. Math.* 46, 1 (1986).
- [10] A. Harten, "ENO Schemes with Subcell Resolution," *J. Comput. Phys.*, V83 (1989), pp.148-184.
- [11] H. Yang, "An Artificial Compression Method for ENO Schemes, the Slope Modification Method," *J. Comput. Phys.*, V89 (1990) pp.125-160.